Liquid-like relaxation in hyperquenched water at ≤140 K

Ingrid Kohl,*[a] Luis Bachmann,[b] Andreas Hallbrucker,[a] Erwin Mayer[a] and Thomas Loerting[ab]

[a] Institute of General, Inorganic and Theoretical Chemistry, University of Innsbruck, A-6020 Innsbruck, Austria. E-mail: ingrid.kohl@uibk.ac.at
[b] Institute of Physical Chemistry, University of Innsbruck, A-6020 Innsbruck, Austria

Micrometre-sized water droplets were hyperquenched on a solid substrate held at selected temperatures between 150 and 77 K. These samples were characterized by differential scanning calorimetry (DSC) and X-ray diffraction. 140 K is the upper temperature limit to obtain mainly amorphous samples on deposition within 16–37 min. DSC scans of glassy water prepared at 140 K exhibit on heating an endothermic step assignable to glass → liquid transition, with an onset temperature (T_g) of 136 ± 2 K on heating at 30 K min^{-1}. For T_g of $\approx$136 K, water relaxes during deposition at 140 K for 16 min, moving towards metastable equilibrium. The apparent increase in heat capacity (ΔC_p) depends, for a given rate of heating, on the rate of prior cooling, and a so-called overshoot develops. 140 K deposits cooled at a rate of 5, 2 or 0.2 K min^{-1} show on subsequent reheating at a rate of 30 K min^{-1} ΔC_p values of 0.7, 1.1 and 1.7 J K^{-1} mol^{-1}. This is consistent with liquid-like relaxation at 140 K, and it indicates that different limiting structures are obtained. When these 140 K deposits are in addition annealed at 130 K for 90 min, after slow-cooling at 5, 2 or 0.2 K min^{-1}, their ΔC_p values on subsequent reheating are similar to those of hyperquenched glassy water (HGW) deposits made at 77 K and annealed at 130 K. Thus, the previous ΔC_p value of 1.6 J K^{-1} mol^{-1} obtained with glassy water samples annealed at 130 K (A. Hallbrucker, E. Mayer and G. P. Johari, *Philos. Mag. B*, 1989, **60**, 179) must be an upper-bound limit because it contains a contribution from an overshoot. The T_g value of 140 K deposits, which had relaxed during deposition towards metastable equilibrium, is within experimental error the same as that of 140 K deposits annealed in addition at 130 K. This contradicts Yue and Angell's (Y. Yue and C. Angell, *Nature*, 2004, **427**, 717) claim for assigning the endothermic step to a sub-T_g peak or a "shadow" T_g. Our new data further support the proposed fragile-to-strong transition on cooling liquid water from ambient temperature into the deeply supercooled and glassy state. We also describe in detail experimental aspects to obtain HGW specimens, show the ultrastructure of the deposits using electron microscopy, and discuss the mechanism of our hyperquenching method.

Introduction

It's being vigorously debated whether glassy water turns on heating between $\approx$140–150 K into a deeply supercooled and highly viscous liquid, or whether it remains glassy until it crystallizes to cubic ice (recently reviewed in ref. 1–3). In the first case the onset temperature of the glass → liquid transition (T_g) is at $\approx$136 K, as we had reported in our previous studies of hyperquenched glassy water (HGW) by differential scanning calorimetry (DSC) heating curves on heating at 30 K min^{-1}.[4–7] In that case measurements of transport and flow properties of the liquid seem possible in order "to clarify the nature of water's low-temperature non-crystalline state".[2] In the second case the glass transition would not be directly observable because it would occur above the crystallization temperature to cubic ice, and water's recently proposed glass transition temperature of 165 ± 5 K by Angell and colleagues would be accessible only indirectly.[1,8,9] These proposals for revising the value of water's T_g to higher temperature and for assigning the endothermic peak at $\approx$136 K to a sub-T_g peak or a "shadow" T_g have been refuted by Johari in several papers,[10–14] and these papers should be consulted for details of the arguments for and against revising water's T_g value.

Here we show by DSC heating curves that hyperquenched water deposited at 140 K behaves as an ultraviscous liquid, its limiting structure depending on cooling rate in a manner predicted by theoretical analysis of liquid-to-glass transition.[15,16] This is consistent with the T_g of $\approx$136 K,[4–7] and with Johari's recent calculation of the dielectric relaxation time of

water of 42 ± 14 s at 136 ± 1 K (ref. 13 and 14; see also ref. 17). A preliminary account of our DSC study has already been published in ref. 18. We further show that the effect of annealing temperature is not compatible with relaxation behaviour of a sub-T_g peak. We then discuss how our new data support the proposed fragile-to-strong transition on cooling liquid water from ambient temperature into the deeply supercooled and glassy state.[19–22] We note that in our opinion the debate on glassy water's T_g value has contributed significantly to our understanding of HGW's low-temperature behaviour, and of that of other liquids hyperquenched into the glassy state.

We also describe in detail experimental aspects of hyperquenching water and aqueous solutions and discuss its mechanism because it may be helpful to other research groups using our hyperquenching method,[23–28] or adapting it.[29–32] Furthermore, Angell and colleagues[1,8,9,33] recently started to hyperquench organic and inorganic liquids into their glassy state and study their DSC scans on reheating in order to account for enthalpy release in HGW.

Experimental

Hyperquenching of μm-sized water droplets

Vitrification of water by so-called hyperquenching of liquid water droplets on a solid substrate was first reported in 1985.[34] The advantage of this method over previously reported methods for vitrifying pure liquid water[35–37] was that it did not
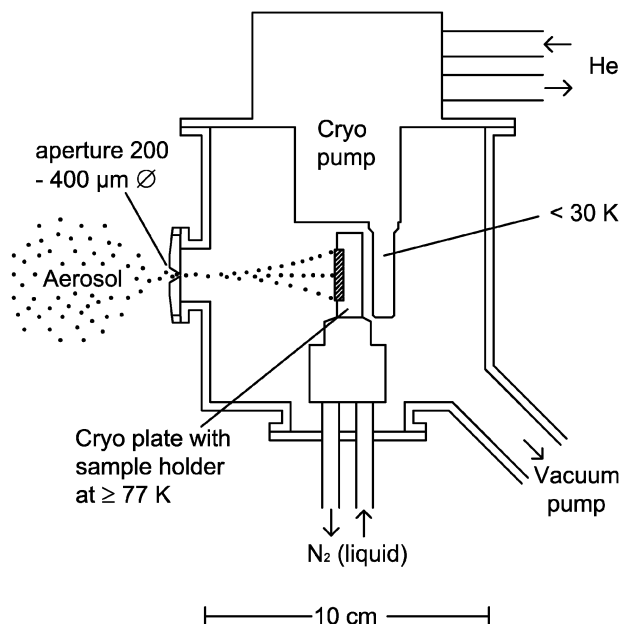

Fig. 1 Schematic diagram of experimental setup for vitrification of micrometre-sized water droplets by "hyperquenching" on a sample holder attached to a cryoplate and cooled with liquid N_2. Aerosol droplets are shown enlarged.

require a liquid cryomedium such as liquid ethane or propane for heat transfer, and therefore, that many subsequent studies by *e.g.* DSC, diffraction and spectroscopy became possible. We describe here the method once more in detail because we had optimized it. The experimental setup is shown in Fig. 1. The vacuum system consisted of a two-stage rotary pump, a turbomolecular pump and a powerful cryopump (*cf.* below) cooled to ≈ 25–30 K. The aerosol is admitted continuously into the high-vacuum system with nitrogen as carrier gas (99.995% pure) through an aperture, where it is accelerated by supersonic flow and deposited on a cooled X-ray sample holder mounted on a cryoplate (made of copper) which was held at a selected temperature. The temperature of the cryoplate was regulated with a thermocontroller (AP Paar, Model TTK-HC) and remained constant within ±0.1 degree. After deposition above 77 K, the deposits were cooled to 77 K, the vacuum broken with gaseous N_2 (99.995%), and the cold X-ray sample holder with cryoplate pulled out of the apparatus and immediately immersed in liquid N_2. All subsequent operations were carried out on samples while immersed in liquid N_2. Samples for DSC studies were taken from the X-ray sample holder outside the area exposed later to X-rays; therefore, samples for X-ray and DSC measurements were from the same preparation. The deposit is obtained in form of a disk-shaped opaque layer which adheres strongly to the sample holder. Thickness of the layer is not uniform, it is larger in the middle. This difference increases with increasing deposition time until the deposit develops a pronounced cone. The layer becomes much more transparent when submersed in liquid N_2 which fills the gaps and cavities between the quenched droplets as shown below in Fig. 2.

Further aspects of the method are described as follows. An aqueous aerosol is produced by ultrasonic nebulization. Droplet size depends *via* an inverse relationship on ultrasonic frequency (eqns. 4.14–4.16 in ref. 38). We use two types of ultrasonic nebulizers routinely for water and dilute aqueous solutions, one operating at 1.7 MHz (HICO Ultrasonat, model 706E) produces, according to company specifications, droplets with a mean diameter of ≈ 5 μm (used for the HGW samples of Fig. 3–5), the other operating at 3 MHz (LKB Instruments, model 108) produces droplets of ≈ 3 μm diameter (used for Fig. 2). The first type is used mainly for H_2O because it is more

convenient to use, the second type for D_2O because it requires much less sample. (We note that these nebulizers don't work for concentrated aqueous solutions and organic solvents, and then a pneumatic nebulizer, *e.g.* a Babington nebulizer type MDSN had to be used). The aerosol is transferred with nitrogen (purity 99.995%) as carrier gas through a silicone tube (1 m long, 20 mm inner diameter) which is cooled with ice water in order to reduce the relative amount of water vapour. Thereafter it is conveyed through an electron microscopic aperture, with 200 or 300 μm diameter (Balzers No. 16 021, 16 022), into the high-vacuum system. The distance between aperture and sample holder is 70 mm. Further important aspects for successful "hyperquenching" of water droplets are: (i) The droplet density of the aerosol. This depends on the flow rate of the carrier gas and on the dosage of water to be nebulized. Small droplet density leads to vaporization of the tiny droplets and increasing deposition of water vapour. This is shown in Fig. 1 and 2 of ref. 39, and it demonstrates how the decoupled OD stretching transition of vapour-deposited amorphous solid water (ASW) centered at 2440 cm^{-1} grows with decreasing droplet density and separates from that of HGW centered at 2416 cm^{-1}. Large droplet density can lead to plugging of the aperture and to increasing amounts of crystalline ice. We found the following parameters optimal for generation of aerosol: for the HICO Ultrasonat nebulizer intensity 6, N_2 carrier gas 2.0 l min^{-1}; for the LKB nebulizer 80% H_2O, 8 l min^{-1}, N_2 carrier gas 2.0 l min^{-1}. A useful criterion for estimation of whether water droplets or mainly water vapour had been deposited is the time it takes for making a deposit with ≈ 1 mm thickness: this requires ≈ 37 (≈ 16) min when using a 200 (300) μm diameter aperture. Deposits of similar thickness but made over hours consist mainly of deposited water vapour. (ii) Low base pressure. For high density free jets and axially symmetric flows, the location of the Mach disk, x_M, depends on the pressure ratio according to eqn (1) (eqn (47) in ref. 40)

$$\frac{x_M}{D_N} = 0.67 \sqrt{\frac{p_0}{p_b}} \qquad (1)$$

where D_N is the nozzle (aperture) diameter, p_0 the source pressure and p_b the base pressure in the vacuum system. Thus, it requires a sufficiently high pressure ratio to obtain supersonic flow immediately downstream of the nozzle throat, and pressure ratios in excess of 10^4 are commonly used.[40]

The effect of base pressure in the vacuum system during continuous deposition of water droplets on a cryoplate is shown in Fig. 3 of ref. 34: this demonstrates that low base pressure of $<10^{-2}$ mbar generates mainly HGW, whereas a base pressure of ≈ 1 mbar gives mainly crystalline ice. Base pressure during deposition was ≈ 0.002 (≈ 0.005) mbar when using the 200 (300) μm aperture. The actual base pressure immediately above the cryoplate could be higher because the probe head of the Pirani instrument was placed ≈ 8 cm from the sample holder. Low base pressure probably acts in two ways. First, for supersonic flow to occur during expansion of a gas through a nozzle into vacuum, the Knudsen number Kn (ratio of mean free path in gas supply to smallest dimension of orifice) has to be <1.[40,41] Important parameters for characterizing supersonic flow in an experiment are the nozzle (our aperture) diameter, d, the ratio of distance between nozzle exit-cryoplate and nozzle diameter, x/d, and the pressure ratio, p_0/p_b, between source pressure, p_0, and the base pressure in the vacuum system, p_b. As p_0/p_b increases, supersonic flow becomes increasingly likely. In our experiments p_0 is atmospheric pressure. Therefore, p_0/p_b increases with decreasing base pressure in the vacuum system during deposition of water droplets, and supersonic flow becomes increasingly possible. A second effect of high base pressure during deposition of water droplets could be that the droplets are
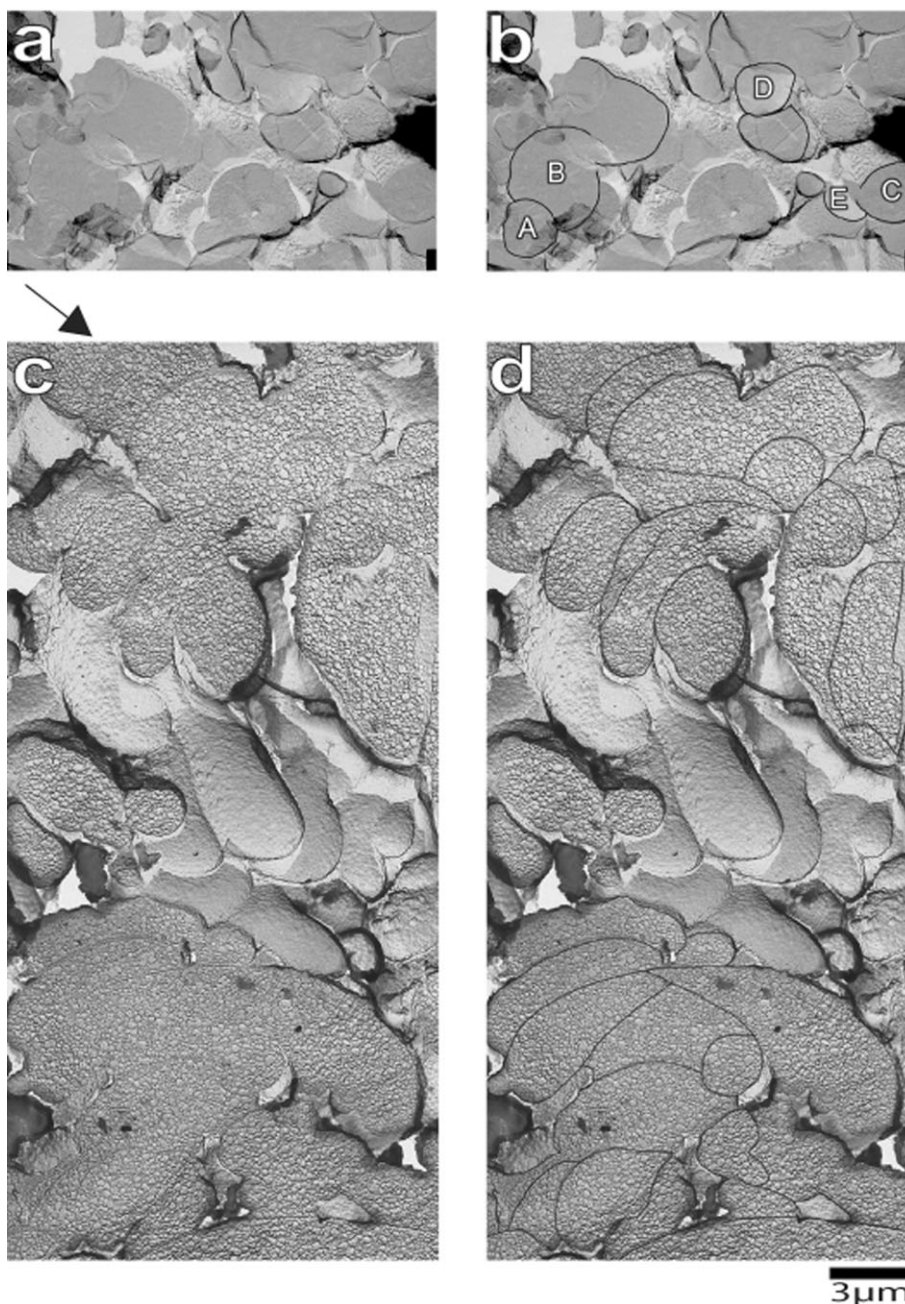
Fig. 2 Ultrastructure of deposits hyperquenched at 77 K and visualized by electron microscopy with the freeze-etching and shadowing technique (*cf*. ref. 44 and 45). (a) A sample of pure HGW was fractured parallel to the specimen support plate (sample holder in Fig. 1). (c) A sample of hyperquenched 10% glycerol in water was fractured vertical to the specimen support plate. Thin faint lines circumscribing in (a) and (c) the boundaries of individual droplets are outlined in (b) and (d). (a) to (d) are shown on the same scale, the bar at the bottom indicating 3 μm. Droplet size of the aerosols for both deposits was ≈3 μm diameter. Note that, by comparison with the bar of 3 μm length, the diameter of the hyperquenched droplets in (a) is also roughly 3 μm. The direction of the aerosol jet is indicated in (c) by the arrow, in (a) it is perpendicular to the fractured plane of the HGW deposit.

precooled slowly already in the gas phase by cold gaseous N_2, and thus, that phase transition to crystalline ice could occur already in the gas phase. For obtaining sufficiently low base pressure during deposition of water droplets through apertures with 200 or 300 μm diameter we used a high-capacity cryopump (Displex cryostat from Air Products, model DE-208L, or a Leybold model RGD 1245) combined with a turbomolecular pump (Leybold, model PT 361). Other pumping systems of high capacity obviously can be used, but we note that the cryopump from Displex, model 202, which is popular in matrix isolation studies, does not have sufficient pumping capacity. For obtaining constant low base pressure for up to 1 h deposition time, it was essential to separate the cryoplate with attached sample holder from the cryopump, by

cooling the cryoplate with cold N_2 as depicted in Fig. 1 (called Method II in ref. 34) even when using a high-capacity cryopump. In order to condense gaseous N_2 most efficiently close to the sample holder, a copper plate with 50 mm diameter (OFHC copper) was attached to the cryotip of the cryopump (shown in Fig. 1). This copper plate was placed behind, and parallel, to the cryoplate with sample holder, with a distance of ≈10 mm, in a way that it extended several millimetres beyond the sample holder. We had also varied the carrier gas and had used gaseous O_2 or Ar instead of gaseous N_2. In these cases much more crystalline ice, up to ≈15%, were obtained than with N_2. This could possibly be caused by changes of the supersonic flow conditions by the heavier carrier gases.
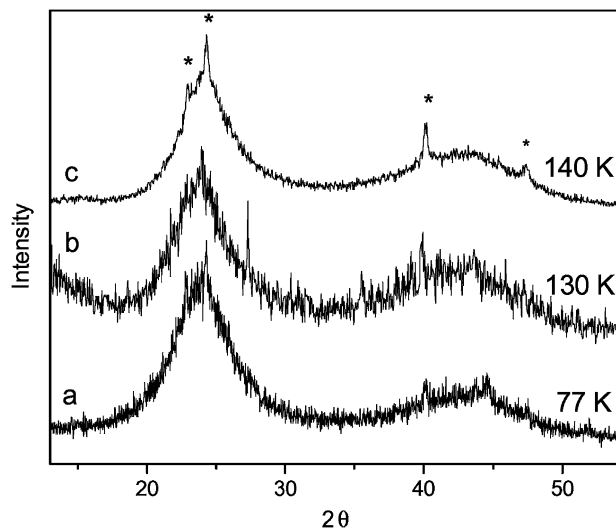
Fig. 3 X-ray diffractograms (Cu Kα) of hyperquenched deposits of water droplets with ≈3 μm diameter and recorded at 113 K: temperature of the substrate during deposition was 77 K for (a), 130 K for (b) and 140 K for (c). Deposition time was 37 min for deposition at 130 and 140 K, and cryoplate with deposit were cooled immediately after deposition to 77 K at a rate of ≈5 K min^{-1}. Asterisks mark bands from crystalline ice.

(iii) Visualization of the quenched droplets is obviously most direct by electron microscopy, as shown below in Fig. 2. However, this method is demanding and requires non-standard instrumentation. A simpler, indirect, method of observing the quenched droplets is by Fourier transform infrared (FT-IR) spectroscopy. IR spectra of quenched micrometre-sized droplets display the Christiansen effect where distortion of IR bands leads to band asymmetry and even shift of band maxima. (see Fig. 1 and 2 in ref. 39). This distortion is absent in vapour-deposited samples, and therefore, qualitative estimation of the relative amounts of ASW and HGW is possible. Distortion of IR spectra in form of a strongly sloping background between 4000 and 3500 cm^{-1} was also observed by droplets of hyperquenched methanol (Fig. 1 in ref. 42) and
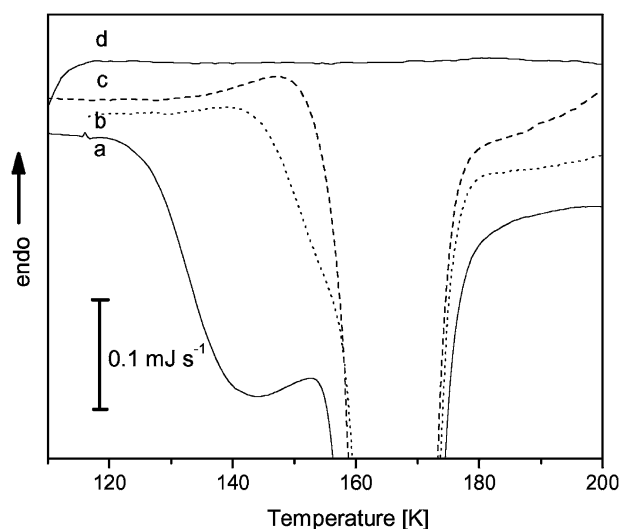

Fig. 4 DSC scans of unannealed HGW samples made by deposition at 77 K (a), 130 K (b) and 140 K (c). Curve (d) is for comparison the scan of a cubic ice sample made by heating HGW, deposited at 140 K, up to 193 K and holding it at 193 K for 5 min. The samples were cooled after deposition at a rate of ≈5 K min^{-1} to 77 K. The scans are normalized with respect to the samples' weights and are drawn on the same scale but are shifted vertically for clarity. The ordinate scale is for 1 mg sample weight. The DSC scans were recorded on heating at 30 K min^{-1}.
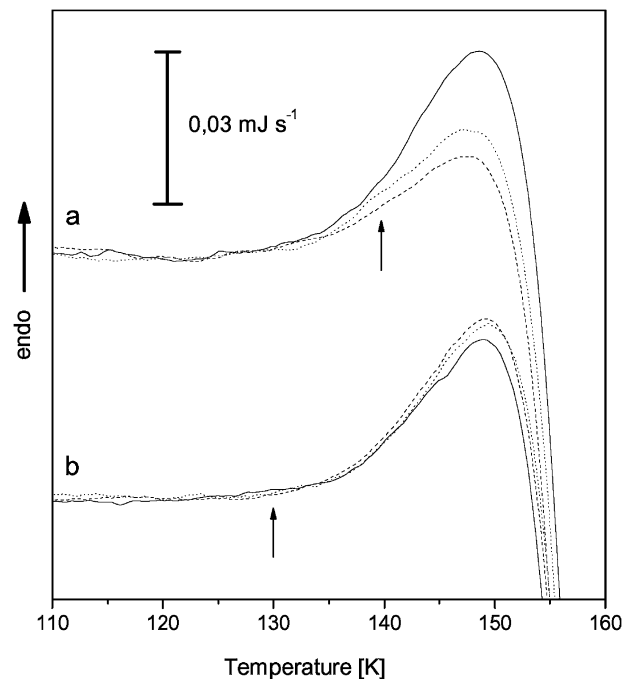

Fig. 5 (a) (top) Effect of cooling rate of unannealed HGW samples after deposition at 140 K for 16 min, on DSC scans recorded on subsequent heating at 30 K min^{-1}: the cooling rate was increased from 0.2 K min^{-1}, to 2, and 5 K min^{-1}, and the corresponding DSC scans are indicated by a solid (0.2 K min^{-1}), dotted (2 K min^{-1}) and dashed (5 K min^{-1}) line. Note the decrease of the height of the endothermic step with increasing cooling rate. The arrow marks the deposition temperature of 140 K. (b). (bottom) Effect of annealing at 130 K for 90 min on HGW samples, after deposition at 140 K for 16 min and cooling at 0.2, 2 and 5 K min^{-1}, on DSC scans recorded on subsequent heating at 30 K min^{-1} (marked as in 5(a)): Note the disappearance of the effect of cooling rate shown above for unannealed samples. The arrow marks the annealing temperature. The scans are normalized with respect to the sample weights and are drawn on the same scale. The ΔC_p values are corrected for 22% ice impurity. The ordinate scale is for 1 mg sample weight. The scans are superimposed at low temperatures. From ref. 18 with changes.

glycerol (Fig. 8(a) in ref. 42). For quenched methanol and glycerol this distortion disappears on heating ≈20 degrees above the onset temperature of their respective glass → liquid transition temperature because of coalescene of the droplets. This temperature region is inserted in Fig. 9 of ref. 42 in form of a so-called supplemented phase diagram. For the quenched water droplets, however, coalescence of the droplets is prevented by the phase transition to ice Ic, and the formed ice Ic shows the same band distortion by the Christiansen effect as the glassy water droplets (see Fig. 3 in ref. 39). Glassy water deposits obtained on quenching of ≈5 μm-sized water droplets made by the HICO Ultrasonat nebulizer were investigated in this manner. Other indirect methods for ensuring deposition of droplets instead of vapors are to add a solute, and to compare the concentration and its distribution in the solution before and after hyperquenching.[34] An EPR spectroscopic study of hyperquenched 0.010 M CuCl$_2$ solution, performed as described in ref. 35 and 43, showed that the solute concentration in the hyperquenched deposit varied between 0.008–0.012 M when using gaseous N$_2$ saturated with water vapour for producing the aerosol, and between 0.01–0.015 M with dry N$_2$ gas.[34]

Ultrastructure of hyperquenched deposits visualized by electron microscopy

An obvious problem with our hyperquenching technique is that the μm sized water droplets will vaporize *in vacuo* at least partially, and therefore, water vapour may be deposited on the

cryoplate besides or even instead of droplets. Our results obtained by FT-IR and EPR spectroscopy of hyperquenched deposits[34,39] have already ruled out that the HGW samples are contaminated by a substantial amount of condensed water vapour. The fraction of simultaneously deposited water vapour depends on droplet density of the aerosol and on its temperature.[39] This fraction had been estimated to be <5% for high aerosol droplet density.[34]

In addition, these results were substantiated by electron microscopy using freeze-etching (for reviews of this technique see ref. 44 and 45). In our case the specimen preparation was as follows: For Fig. 2(a) a sample of pure HGW on a metal support plate was transferred from liquid N_2 onto the cold stage of a freeze-etching apparatus BA 400T and evacuated to 10^{-6} mbar. The specimen was then fractured parallel to the support plate (sample holder in Fig. 1) in a freeze etching apparatus BA 400T at 165 K with a liquid N_2 cooled microtome and immediately shadowed with Pt/C and backed with a carbon support film. These freeze etching conditions lead to formation of cubic ice from HGW. Finally the replica was floated on water and mounted on specimen grids for electron microscopy.

In the case of Fig. 2(c) a sample of hyperquenched 10% glycerol in water was fractured in the direction of the jet stream, that is vertical to the specimen support plate in Fig. 1. For this, the sample had to be glued in this orientation onto the specimen holder of the freeze-etching device at a temperature of 180 K.[46] The specimen was then fractured at 170 K and, after an etching period of 1 min to allow the sublimation of a thin ice layer, was shadowed with Pt/C and processed as for Fig. 2(a).

The electron micrograph of the replica in Fig. 2(a) shows smooth fracture planes through the round droplets of the originally hyperquenched water which became crystallized at the temperature of freeze fracturing and replication. In addition Fig. 2(a) shows unfractured areas which are located at a lower level than the fracture plane. On these areas frozen droplets can be seen which form the walls of the gaps and cavities which became exposed by the fracturing process. The presence of such cavities in the sample causes the opaque appearance of the HGW layers as mentioned above. The surface of the unfractured droplets is speckled with very small particles consisting of frozen water vapour. The growth rate of the HGW layer is estimated from sample thickness and deposition time as ≈ 1 μm per second while the droplets solidify in less than a millisecond (see below). Thus the solidified drops on front of the growing layer are exposed to the residual water vapour until they are covered by another droplet. This may last for seconds as the droplets arrive on the deposit stochastically and the surface of gaps and cavities may be exposed to water vapour even longer until they are sealed by the growing layer. Therefore, it seems reasonable to assume that the small particles on the native surface of the cavity walls are indeed clusters of frozen water vapour.

The hyperquenched glycerol solution shown in Fig. 2(c) had to be warmed up to 180 K during specimen preparation. Therefore crystallisation of the water and phase separation of glycerol and ice occurred in the sample. The size of the ice compartments are in the order of 5–20 nm. On the fracture plane the ice in the fractured compartments sublimated during the etching time while the glycerol remained, resulting in a densely dimpled appearance of the surface. As in Fig. 2(a) fracturing also opened cavities in the sample and thereby exposed the walls formed by the frozen droplets. In this specimen the surface of these droplets appears bumpy with little elevations of the same size as the ice compartments. The very small particles seen on the cavity walls in Fig. 2(a) are absent because the frozen vapour sublimated during sample preparation and etching.

On both electron micrographs very thin faint lines can be seen on some areas of the fracture plane while they are absent on other domains. For clarity these lines are enhanced in Fig. 2(b) and 2(d). These lines obviously circumscribe the boundaries of the individual droplets in the deposit and must be caused either by some kind of interlayer between the droplets or by some specific surface properties of the solidified and/or of the liquid droplets.[47] A feasible explanation could be the condensation of water vapour on the surface of solid droplets within the time period between solidification and being covered by an incoming droplet of the aerosol. As already discussed, this time period can vary from milliseconds to seconds and accordingly alters the amount of condensate. The physical-chemical properties of the condensed vapour are definitely different from those of quenched or liquid water. Surface active substances in the liquid may also cause boundary lines between the solidified droplets. However, the deposit shown in Fig. 2(a) consists of pure water. Besides, if surfactants are involved all the droplets of a deposit should be outlined.

In any case, these lines can give us some information on the mechanism of hyperquenching. On sections or fracture faces parallel to the specimen support plate, that is vertical to the direction of the jet, the outline of the droplets is circular but frequently intersected by other circles. A good example is seen on the lower left corner of Fig. 2(b) where a circle with a diameter of 2 μm, designated with (A), intersects a circle (B) with a diameter of 4 μm. The droplets can, of course, be much larger then their diameter observed on a fracture plane but it is obvious that droplet A was already solidified when it was hit and partially surrounded by the liquid droplet B. The droplets C, D and E are partially fractured and show in parts their original surface of the cavity wall. Droplet C is elongated approximately in the direction of the jet.

The deformation of the liquid droplets by the impact on the solid surface of the deposit is better seen on the cross section of the sample vertical to the specimen support plane, that is parallel to the direction of the aerosol jet (indicated by lines in Fig. 2(d)). The direction of the jet is indicated on Fig. 2(c). The central area in Fig. 2(d) shows the inside wall of a cavity where the droplets are elongated in the direction of the jet. The outlined droplets in the fracture plane indicate the degree of spreading and flattening from the impact until solidification.[48–51] The fracture plane shows how densely the droplets are stacked on top of each other and how they get elongated in the direction of the jet at the edge of the cavity. The smallest radius of the half circles at the border of the flattened droplets on the cross section is approximately 1.5 μm. The maximal "thickness" of the flattened droplets is about 3 μm and their maximal "length" is about 5–6 μm. On Fig. 2(c) only droplets of glycerol solution are seen and no droplets or large clusters of condensed water vapour show up.

Differential scanning calorimetry and X-ray diffraction

A differential scanning calorimeter (model DSC-4, Perkin-Elmer) with a self-written computer program was used. After heating each sample up to the melting point and recording its DSC scan, a second heating scan of now ice Ih was recorded and subtracted as base line from the first scan. We believe this to give a more accurate subtraction of base line than the subtraction of a second scan with empty sample pans used routinely in our previous DSC studies.[5,7,52,53] This type of subtraction removes a slight curvature intrinsic in the baseline of the instrument. Between 14 and 23 mg sample were transferred under liquid N_2 into stainless steel capsules with screwable lids. DSC scans were recorded on heating at 30 K min^{-1} from 93 to 278 K. The mass of each sample was obtained via the melting endotherm of ice, by using the value of 6.012 kJ mol^{-1} as heat of melting. For Fig. 4 and 5 the percentage of crystalline ice impurity was determined by comparing the heat

Table 1 Effect of cooling rate of unannealed 140 K deposits on ΔC_p values

Number of batches	Number of samples	Percentage amorphous	Cooling rate/K min^{-1}	ΔC_p/J K^{-1} mol^{-1}	T_g/K	Width/K
3	18	81 ± 4	0.2	1.7 ± 0.3	135 ± 1	12 ± 1
2	9	84 ± 4	2	1.1 ± 0.2	136 ± 2	11 ± 2
2	9	81 ± 4	5	0.7 ± 0.1	135 ± 1	11 ± 1

[a] For Tables 1 and 2: T_g is the onset temperature of the endothermic feature, ΔC_p the apparent increase in heat capacity in the glass → liquid transition region. Cooling rate refers to cooling of the sample from 140 K to 77 K, after hyperquenching at 140 K.

of crystallization of HGW → ice Ic with the value of −1.43 kJ mol^{-1} for 100% HGW (*cf.* Table 1 in ref. 7) obtained from HGW samples deposited at 77 K and annealed at 130 K. That value had been corrected for 5% crystalline ice impurity in the same manner reported before for unannealed HGW.[52] Hyperquenched samples of ≈1 mm thickness were obtained either after 16 min deposition time through a 300 μm diameter aperture or after 37 min through a 200 μm diameter aperture. The percentage of amorphous ice in these samples was in the first case 82 ± 4% (from 7 batches and 57 samples, used for Fig. 5), and in the second 79 ± 7% (from 4 batches and 12 samples, used for Fig. 4). The DSC instrument was calibrated with cyclopentane.

X-ray diffractograms were recorded on a diffractometer in θ–θ geometry (Siemens, model D 5000, Cu-Kα), equipped with a low-temperature camera from Paar. The sample plate was in horizontal position during the whole measurement. Installation of a "Goebel" mirror allowed to record small amounts of sample without distortion of Bragg peaks. For Fig. 3 percentage of crystalline ice in the HGW samples was determined as described in ref. 54.

Results

Fig. 3 shows X-ray diffractograms of deposits of hyperquenched ≈3 μm-sized water droplets which were recorded at 113 K. For Fig. 3(a) the sample was made by droplet deposition at 77 K, for Fig. 3(b) and 3(c) by deposition at 130 K and at 140 K. The latter two samples were cooled immediately after deposition at a rate of ≈5 K min^{-1} to 77 K in order to avoid further transition of HGW to ice Ic. The X-ray diffractogram of Fig. 3(a) contains only a small amount of crystalline ice of ≈ ≤5%, which is seen most clearly by the weak sharp peak at $2\theta \approx 40°$. This small amount of crystalline ice forms partly on condensation of water vapour on the quenched droplets during sample preparation (see footnote 17 in ref. 55). For the samples used for Fig. 3(b) (130 K) and 3(c) (140 K) the amount of crystalline ice was determined by DSC as 4 ± 1% and 22 ± 8%. Mean values for crystalline ice impurity are 8 ± 5% for deposition at 130 K (from three batches and seven samples), and 21 ± 7% for deposition at 140 K (from four batches and twelve samples), both for 37 min deposition time. It is important to note that within the relatively large standard deviation the method is reproducible for a given deposition temperature and time with respect to the percentage of crystalline ice impurity.

Fig. 4 shows DSC scans of unannealed HGW samples which were prepared by deposition at 77 K (a), 130 K (b) and 140 K (c), cooled immediately after deposition to 77 K at a rate of ≈5 K min^{-1}, and subsequently heated at a rate of 30 K min^{-1} for

recording their DSC scans. Curve (d) is for comparison the DSC scan of a sample of cubic ice which was obtained from HGW by heating up to 193 K. In the latter DSC scan the thermal features observable in scans (a) to (c) are absent. The broad exotherm in curve (a) above ≈120 K arises from the rapid and spontaneous enthalpy relaxation to a structural state of lower enthalpy and free energy at $T < T_g$. It masks the weak endothermic feature attributed to water's glass → liquid transition.[4–7] The exothermic feature is very weak in curve (b), and it starts at ≈140 K. In curve (c), the deposit made at 140 K, it is completely absent and an endothermic feature is observed instead.

Fig. 5(a) (top) shows the effect of cooling rate of unannealed HGW samples after deposition at 140 K for 16 min, on DSC scans recorded subsequently on heating at 30 K min^{-1}. The height of the endothermic step decreases with increasing cooling rate from 0.2 K min^{-1} (solid) to 2 (dotted) and 5 K min^{-1} (dashed). Several other samples were studied in the same manner, and Table 1 lists the apparent ΔC_p and T_g values and the width of the glass softening range. The ΔC_p values are corrected for the amount of crystalline ice contained in the samples. We emphasize that the ΔC_p decrease with increasing cooling rate is not caused by a shift of the onset of crystallization to lower temperatures.

We have further investigated the effect of annealing on samples of HGW obtained by deposition at 140 K, and cooled thereafter immediately at a rate of 0.2, 2 or 5 K min^{-1} to lower temperatures. The samples were subsequently annealed in the DSC instrument at 130 K for 90 min, cooled to 93 K, and finally heated from 93 to 278 K at a rate of 30 K min^{-1} and their DSC scan recorded. This annealing temperature and time was chosen because these were used in most of our ealier DSC studies of HGW samples deposited at 77 K.[4–6] Fig. 5(b) (bottom) contains DSC scans of HGW samples annealed in this manner, which had been prepared by deposition at 140 K and subsequent cooling at a rate of 0.2, 2 and 5 K min^{-1}. Table 2 lists for additional annealed samples the apparent ΔC_p and T_g values and the width of the glass softening range. The ΔC_p values are corrected for the amount of crystalline ice contained in the samples. The dependence of the apparent ΔC_p value on cooling rate, which is apparent in Fig. 5(a) (top) and Table 1, disappears on annealing at 130 K (*cf.* Fig. 5(b) (bottom) and Table 2). Once the samples had been annealed at 130 K, no effect of cooling rate could be observed in the DSC scans recorded on subsequent heating within the experimental error.

Discussion

Water's calorimetric glass → liquid transition had previously been determined by DSC on heating glassy water samples

Table 2 Effect of annealing at 130 K for 90 min on glass → liquid transition parameters of HGW samples hyperquenched at 140 K

Number of batches	Number of samples	Deposition temperature/K	Percentage amorphous	Cooling rate/K min^{-1}	ΔC_p/J K^{-1} mol^{-1}	T_g/K	Width/K
2	5	140	83 ± 2	0.2	1.3 ± 0.2	135 ± 2	12 ± 2
2	9	140	82 ± 2	2	1.3 ± 0.2	137 ± 1	11 ± 1
2	7	140	82 ± 3	5	1.5 ± 0.1	136 ± 1	12 ± 1
3	13	77	94 ± 5	≈10^6–10^7 K s^{-1}	1.3 ± 0.2	136 ± 2	11 ± 2

made by "hyperquenching" micrometre-sized water droplets on a cryoplate held at 77 K, and by prior removal of the broad exotherm from enthalpy relaxation *via* annealing at 130 K.[4–7] On heating annealed HGW at a rate of 30 K min^{-1}, T_g is ≈ 136 K (≈ 132 K on heating at 10 K min^{-1}, ref. 23), the temperature range (ΔT) is 12 K, and ΔC_p is ≈ 1.6 J K^{-1} mol^{-1}.[4–7] The weak endothermic increase in C_p is followed by the intense exothermic feature from the beginning of crystallization to ice Ic. Similar behaviour had been observed in DSC scans of rapidly quenched metals and alloys.[12,56,57] The exothermic feature masks the C_p curve of the supercooled liquid following the glass → liquid transition which is observable in less rapidly crystallizing glasses. The apparent peak of the T_g endotherm is therefore an artifact from superposition of the crystallization exotherm on the glass-softening endotherm, and ref. 12 should be consulted for examples of this behaviour and criteria for distinguishing apparent T_g peaks and sub-T_g peaks. Thus, the end temperature of HGW's glass → liquid transition and the C_p value at this temperature are not directly observable.

DSC scans of HGW samples deposited at 77 or 130 K (Fig. 4(a) and 4(b)) show pronounced differences whereas the broad peaks in the X-ray diffractograms (Fig. 3(a) and 3(b)) are undistinguishable. The broad exotherm in the DSC scan of HGW deposited at 77 K (Fig. 4(a)) above ≈ 120 K arises from the rapid and spontaneous enthalpy relaxation to a structural state of lower enthalpy and free energy at $T < T_g$.[4–7,58] This exothermic feature is very weak in the DSC scan of the HGW sample made by deposition at 130 K (Fig. 4(b)), and it starts at ≈ 140 K. Thus HGW had already relaxed to a large part during its deposition at 130 K to a structural state of lower enthalpy and entropy. Enthalpy relaxation in a rapidly cooled glass normally involves densification of its structure.[59] HGW is an exception and a decrease of its density is expected to occur because water's coefficient of thermal expansion is negative below 273 K.[60] It is conceivable that these structural differences between HGW samples deposited at 77 or 130 K become observable in diffractograms of high-quality.

Exothermic features from enthalpy relaxation are absent in the DSC scan of water droplets deposited on a cryoplate held at 140 K (see Fig. 4(c)). Therefore, water's glass → liquid transition can be studied in these samples without prior annealing,[4–7] and the effect of cooling rate can be investigated and discussed with respect to relaxation as shown below.

Relaxation at 140 K is liquid-like

A central question of our DSC study is whether the water droplets hyperquenched on a cryoplate held at 140 K for a given time (which is 16 min for the samples made for Fig. 5) are in metastable equilibrium and thus can be considered as a highly viscous liquid. The structural relaxation time, τ_s, calculated from a DSC scan obtained by heating at a rate of 30 K min^{-1} is ≈ 70 s at T_g, and ≈ 7 s at the midpoint temperature, T_{mp}, of the glass transition endotherm.[61] Johari (footnote 35 in ref. 13) includes in a recent estimation of τ_s at T_g both the non-exponentiality of structural relaxation and the structure dependence of τ_s, and points out that τ_s at T_g should be revised for heating at 30 K min^{-1} from ≈ 70 s to ≈ 33 s. The deposition temperature of 140 K is close to T_{mp} of water's glass transition region estimated as 142 K.[4–7] Therefore, the sample made at 140 K within 16 min by continuous deposition of water droplets should to a large part have attained metastable equilibrium. We will show in the following that the DSC features of these deposits depend on cooling rate in a manner which is consistent with liquid-like behaviour.

"When a liquid is cooled through the glass transition region, it reaches a temperature at which the rate of structural relaxation becomes too slow to be detected experimentally. The limiting structure obtained on cooling may be characterized in terms of a limiting fictive temperature, T'_f, which depends on

cooling rate."[15,16,62,63] Moynihan *et al.*[15] have rederived Ritland's[64] prediction of the dependence of T'_f on cooling rate by using a set of assumptions which allow for the "memory effect". T'_f decreases with decreasing cooling rate. In DSC studies decreasing T'_f becomes experimentally observable on subsequent reheating at a constant rate "mainly as an increase in the magnitude of the heat-capacity maximum", or a so-called overshoot (*e.g.* see Fig. 4 in ref. 15) This overshoot arises when the ratio of the heating to cooling rates is greater than unity and, for a given heating rate, it becomes increasingly pronounced with decreasing cooling rate.[15,63,65] Examples for this type of behavior are shown by a borosilicate crown glass,[15] by glassy As$_2$S$_3$ and B$_2$O$_3$,[62,63] and by glassy polystyrene.[66]

This is also the behaviour shown by the DSC scans of HGW deposited at 140 K (see Fig. 5). Table 1 lists the apparent increase in heat capacity, ΔC_p, with decreasing cooling rate from 0.7 J K^{-1} mol^{-1} on cooling at 5 K min^{-1}, to 1.1 and 1.7 J K^{-1} mol^{-1} on cooling at 2 and 0.2 K min^{-1}. Thus, we conclude that with decreasing cooling rate T'_f decreases and, on subsequent reheating and recording the DSC scan, an overshoot becomes increasingly pronounced. Table 2 shows that these differences between the ΔC_p values disappear when HGW samples cooled at these three rates had been annealed in addition at 130 K for 90 min before their DSC scans were recorded on heating. Accordingly, the same T'_f value had been attained in these glasses after annealing. Table 2 contains also the ΔC_p value of a HGW sample deposited at 77 K. This value is slightly lower than that of 1.6 J K^{-1} mol^{-1} reported before.[4–7] This could be caused by the different, and improved, method of subtraction of a base line applied here (*cf.* Experimental). It follows from the effect of cooling rate and of annealing reported here that the ΔC_p increase of *annealed* HGW samples (*cf.* Fig. 5(b)) and ref. 5) contains contributions from an overshoot, and that the "true" ΔC_p value is lower, possibly approaching the ≈ 0.7 J K^{-1} mol^{-1} value obtained on cooling unannealed samples at 5.0 K min^{-1}. This is significant for estimations of the path liquid water takes on cooling into the glassy state whenever the ΔC_p value enters in the calculations.[5,67–72] Our observation of liquid-like relaxation of HGW samples deposited at 140 K is consistent with Johari's recent calculation of the dielectric relaxation time of water of 42 ± 14 s at 136 ± 1 K.[13,14] It is further consistent with reports by Kay and colleagues[73–76] who had studied the isotope exchange dynamics in the related ASW.

Decrease of T'_f with decreasing cooling rate has also an effect on the T_g value obtained on subsequent reheating but these changes are much more difficult to observe and quantify than the increase in the overshoot.[15,62,63] The expected behaviour is, for a given rate of heating, decrease in T_g with decreasing cooling rate (see Fig. 4 in ref. 15). On heating at 10 K min^{-1}, the onset temperature of the endotherms for glassy propylene glycol and two of its polymers obtained by hyperquenching is within 0.7 K of the corresponding temperature of the glass obtained by cooling the liquid at 10 K min^{-1} (*cf.* Figs. 1–3 in ref. 65). This T_g difference of 0.7 K would not be recognizable in the DSC scans of glassy water samples because their thermal effects in the glass transition region are much weaker than those of propylene glycol and its polymers. Since T_g in our DSC scans can only be reproduced to an accuracy of 1–2 K, we do not expect to be able to resolve a shift of the order of ≈ 0.7 K.

A difference between the studies of the effect of cooling rate reported in ref. 15, 62, 63 for typical glass formers, and that reported here for HGW deposits at 140 K, is that the former studies started cooling from a fully equilibrated liquid. However, for the HGW samples made at 140 K by continuous deposition of droplets for 16 min, the quenched droplets spend between 16 and 0 min at 140 K before cooling at a controlled rate is started. Thus, equilibration of the quenched droplets varies depending on the time spent at 140 K, and a distribution

of structural states is obtained. We emphasize that we have kept the experimental parameters for formation of HGW deposits at 140 K as identical as possible, and thus are confident that the effects depicted in Fig. 5 (top) and listed in Table 1 are attributable to variation of the cooling rate, and not to variation in deposition conditions.

Glassy water's endotherm is not a sub-T_g peak

Recently Yue and Angell[9] compared the behaviour of HGW to that of hyperquenched inorganic glasses and claimed that water stays glassy as it heats up to its crystallization point. They concluded that the endothermic step observable in DSC scans of HGW should be assigned to a sub-T_g peak or a "shadow glass transition" whereas the "real" glass transition of water is at much higher temperature "and cannot be probed directly".[9] They also find a "hidden" glass-to-liquid transition at about 169 K.

A sub-T_g peak can arise as a broad endothermic peak in DSC heating scans of the isothermally annealed state of hyperquenched as well as slow-cooled glasses. "On further heating, a broad exothermic minimum appears and finally the onset of its T_g-endotherm appears" (reviewed in ref. 11). Johari[11] summarized the several criteria for such a sub-T_g peak and the differences to a T_g-endotherm. Three of these are that annealing is necessary for observing the sub-T_g peak, that the onset temperature of the sub-T_g peak (T_{onset}) is the same as the annealing temperature (T_{ann}), and that an increase in T_{ann} for a fixed annealing time (t_{ann}) increases T_{onset} of the sub-T_g peak, its height, area, and its temperature.

The latter effect of T_{ann} on T_{onset} of a sub-T_g peak at a fixed t_{ann} allows to differentiate most clearly between a sub-T_g peak and a T_g-endotherm. Our DSC studies of hyperquenched propylene glycol have shown that the effect of T_{ann} on T_g is only slight (cf. Fig. 4 in ref. 65). Yue and Angell[9] point out that "shadow transitions (prepeaks) increase in both transition strength and onset temperature with increase in T_{ann} values" (cf. legend to Fig. 3). They show in their Fig. 3a DSC difference curves of a hyperquenched inorganic glass used as a model system for HGW that for T_{ann} of 993 K T_{onset} of the sub-T_g peak (called $T_{g,shadow}$ in ref. 9) is at 1063 K whereas for T_{ann} of 1033 K it is at 1120 K. Thus, increase of T_{ann} by 4.0% causes increase of T_{onset} by 5.4%. In contrast to that, onset temperature of HGW's weak endothermic step remains at ≈136 K, despite an increase of T_{ann} from 130 K (Fig. 5b) to 140 K (Fig. 5a) by 7.7%! This contradicts Yue and Angell's[9] claim for assigning HGW's endothermic step to a sub-T_g peak or a "shadow" T_g at 141 K. We further note that Yue and Angell based their assignment of HGW's endotherm to a "shadow" T_g at 141 K on a DSC scan shown in our previous study (cf. Fig. 3b in ref. 9, and Fig. 1/140 K in ref. 54). This DSC scan was recorded at the very beginning of our study of 140 K deposits. At that time we were not aware of the importance of the cooling rate in order to achieve reproducible results, and so the cooling rate was not controlled. Furthermore, for this very weak thermal effect we consider it essential to use the mean values as we have done in this study in our Tables 1 and 2, rather than a single value. Additional arguments against assignment of HGW's endotherm to a sub-T_g peak can be found in ref. 10–13.

Fragile-to-strong transition on cooling liquid water?

In Angell's classification scheme, "strong" liquids exhibit Arrhenius behaviour of the temperature dependence of their viscosities, whereas liquids exhibiting marked deviations from Arrhenius behaviour, with the viscosity rising faster as temperature gets lower, were termed "fragile".[1,19–21,77,78] "Strong liquids, such as the network oxides SiO_2 and GeO_2, have tetrahedrally coordinated structures that resist thermal degra-

dation. When heated across the glass transition, their short- and intermediate-range order tends to persist. This structural stability is reflected in the small heat capacity and thermal expansion coefficient changes that accompany the vitrification of strong liquids. In contrast, any remnants of the structure in which a fragile liquid is trapped below T_g disappear rapidly upon heating above T_g. This is reflected in relatively large changes in heat capacity and thermal expansion coefficient at T_g".[78]

Thus, the ΔC_p change at T_g is a good indicator for strong or fragile behaviour. Whereas water at temperatures down to 238 K is the most fragile liquid of all (cf. Fig. 1 in ref. 19), its ΔC_p increase at T_g of ≈1.6 J K^{-1} mol^{-1} obtained by DCS heating curves[5–7] is much less than that predicted by extrapolations of ΔC_p data from slow-cooled concentrated binary aqueous solution glasses.[79] This apparent contradiction had been attributed to water changing from a fragile liquid to a strong liquid as temperature decreases during hyperquenching (or as the binary solutions change composition during dilution at low temperature).[19] We show in this study that the previous ΔC_p value of 1.6 J K^{-1} mol^{-1} obtained with glassy water samples annealed at 130 K (ref. 5–7) must contain a contribution from an overshoot, and that water's "true" ΔC_p increase at T_g must be lower, possibly approaching the ≈0.7 J K^{-1} mol^{-1} value obtained on cooling at 5.0 K min^{-1}. A lower ΔC_p value is consistent with increasingly "strong" behaviour of deeply supercooled water[19,20,77,78] and thus, our new data support the postulated fragile-to-strong transition on cooling liquid water from ambient temperature into the deeply supercooled and glassy state.[19–22] We note that Angell and colleagues[80] recently concluded from dielectric studies that their "findings eliminate "ultraviscous fragile liquid" as a possible description of water between 136 K and crystallization, but leave "ultraviscous strong liquid" a possibility to be considered".

Mechanism of hyperquenching

Fig. 3 shows that variation of the substrate temperature between 77 K and 130 K has no effect on the percentage of crystalline ice formed. Thus, the average cooling rate obtainable on hyperquenching μm-sized water droplets can depend only to a minor extent on the substrate temperature for the temperature range 77 to 130 K. This is a characteristic of so-called ideal cooling. We note that flattening of the droplets observable in Fig. 2(c) proves that they must have still be liquid when hitting the cryoplate and the already quenched droplets.

Ruhl[81] has analyzed heat transfer in splat cooling of liquid metals and alloys on a solid substrate. He concluded that splat thickness (d) and heat transfer coefficient (h) were the most important variables. Ruhl's somewhat simplified, but elucidating calculations are, in principle, also applicable to aqueous specimens. The most important difference is that water conducts heat more than 100 times more slowly than iron used in Ruhl's analysis.[81] Here we use his analysis for discussion of hyperquenching of micrometre-sized water droplets at 140 K. To obtain a HGW deposit of ≈1 mm thickness, several hundreds of micrometre sized droplets have to be deposited onto each other. This can occur via deposition of incoming droplets on top of already deposited droplets, or into interstices of various shapes between deposited droplets, and Fig. 2(a) and 2(c) show examples for each of these cases. For the first layer of quenched droplets on the substrate (i.e. the X-ray sample holder), the heat flow can be subdivided into the transport within the droplet hitting the substrate, heat transport between the droplet and the substrate, and within the substrate. For the successive layers of quenched droplets heat transfer is more complicated, and heat transfer beween incoming droplet and deposit of droplets, transport within the deposit and heat transfer between deposit and substrate have to be considered in addition.[81,82] According to Ruhl[81] "the

criterion for determining which type of cooling prevails in a particular instance was found to be the quantity hd/k_s ($=Nu$, the Nusselt or Biot number) where k_s is the thermal conductivity of the splat material", h the heat transfer coefficient and d the sample thickness.

(i) For $Nu \geq 30$, optimal or "ideal" cooling of a droplet is obtained and the thermal contact between droplet and substrate is effectively perfect, that is when h becomes very large. This can only be obtained when the conduction of heat through the droplet-deposit-substrate contact area and within the deposit-substrate occurs much faster than within the incoming droplet, and it leads to a pronounced temperature gradient within the droplet. For this case the cooling rate is determined by the droplet, and it cannot be increased any more by further technical improvements such as using a substrate with still higher thermal conductivity or lower substrate temperature.

(ii) For $Nu < 0.015$, Newtonian cooling occurs where h is small, the thermal gradient in the droplet is negligible and the cooling is completely interface controlled.

(iii) Intermediate cooling occurs for situations between (i) and (ii).

Ruhl's[81] calculations demonstrated that for ideal cooling the substrate temperature has no effect on the average cooling rate, and his experimental findings agreed with these calculations: "for metastable structures which could be preserved at room temperature, no effect was noted upon changing the substrate temperature to $-190 \, °C$".[81]

$Nu \geq 30$ characterizes ideal cooling and it becomes, for a given value of k_s, increasingly easy to achieve by increasing d. In that case it is easy to achieve ideal cooling of a large sample of water with conventional cooling methods since cooling is then limited by heat flow within the sample. However, the second relationship to consider here is the dependence of the cooling rate on d: for ideal cooling the cooling rate varies inversely as d^2, and therefore, only low cooling rates are achievable for large values of d. Uhlmann's[83] estimation of the critical cooling rate needed to avoid detectable crystallization on quenching liquid water was based on hypothetical viscosity-temperature relation, and it predicted $\approx 10^7 \, K \, s^{-1}$ for a glass with an obtainable thickness of $\approx 1 \, \mu m$. Bald's[84] estimation of the critical cooling rate was based on a theoretical model of critical heat flux, and it predicted complete vitrification for cooling rates in excess of $\approx 3 \times 10^6 \, K \, s^{-1}$, which can be achieved for droplets up to $\approx 3.6 \, \mu m$ diameter. Bald's value of the minimum critical cooling rate of $\approx 3 \times 10^6$ $K \, s^{-1}$ is close to our estimation of $\approx 10^6$–$10^7 \, K \, s^{-1}$.[82,85] Since for ideal cooling the cooling rate varies inversely as d^2, this critical cooling rate becomes increasingly achievable as sample size decreases and, as shown by Dubochet and coworkers by their thin-film method developed for applications in cryo-electron microscopy,[36,86] "vitrification becomes easy when the dimension of the sample reaches the size required for observation in transmission electron microscopy" which is less than 1 μm thickness.[86]

The upper limit of water sample thickness which can be vitrified completely by hyperquenching, has not yet been determined in the same manner as shown in Fig. 2 and 3 for $\approx 3 \, \mu m$-sized droplets, by determining the diameter of the quenched and flattened droplet, and the percentage of HGW and crystalline ice. In our experience hyperquenching of ≈ 5 μm-sized droplets, which were produced by an ultrasonic nebulizer operating at 1.7 MHz, works in the same manner as that of 3 μm-sized droplets by producing only $\approx \leq 5\%$ crystalline ice on deposition at 77 K (cf. Fig. 3 and 4). Hyperquenching of larger droplets into the glassy state was attempted with droplets produced by an ultrasonic nebulizer operating at 105 kHz.[34] This frequency is supposed to produce droplet sizes of $\approx \leq 25 \, \mu m$ diameter.[38] The deposit consisted largely of crystalline ice (its X-ray diffractogram was similar to

that in Fig. 3(b) of ref. 34) However, in this case we do not know the distribution of droplet sizes. A reliable value for the maximal sample thickness which can be vitrified is only obtainable by an experiment in the same manner shown in Fig. 2 and 3 for $\approx 3 \, \mu m$-sized droplets. Dubochet and McDowall[36] reported that pure liquid water can only be vitrified for layers up to 1 μm. However, their method involves quenching of thin water films in liquid propane or ethane. Therefore, the mechanism is expected to differ and these values may not be applicable to our hyperquenching method.

HGW samples obtained by deposition between 77 and 130 K contain $\leq \approx 5\%$ crystalline, mainly cubic, ice. This amount does not depend on sample thickness; HGW films of several μm diameter used for FTIR spectroscopic studies in transmission[60,87] and HGW deposits of up to $\approx 2 \, mm$ thickness used for diffraction and DSC studies contained similar fraction of crystalline ice. Thus, heat transfer across the already deposited hyperquenched droplets does not decrease with increasing sample thickness. Part of this crystalline ice is formed via deposition of water vapour (cf. footnote 17 in ref. 55), and the value of $\approx 95\%$ vitrified droplets is thus a lower limit. The remaining few% of crystalline ice impurity could either be distributed evenly among all deposited droplets, or concentrated on a few droplets quenched at a lower rate of cooling. We consider the latter more likely because our FT-IR spectroscopic study of the crystallization kinetics of HGW showed that annealing of HGW at 130 K for 2 hours accelerates remarkably its subsequent isothermal crystallization at 144 K (cf. Fig. 3 in ref. 60). This had been attributed to the growth of nuclei during annealing. No such effect on annealing is expected when each quenched droplet had contained already some crystalline ice. We assume that the droplets quenched at a lower rate of cooling are those that hit some of the interstices formed by already deposited droplets and thus have reduced thermal contact for optimal heat transfer.

HGW samples deposited at 140 K contain more ice, and the percentage of HGW decreases slightly from $82 \pm 4\%$ after 16 min deposition time, to $79 \pm 7\%$ after 37 min. This is attributed to partial crystallization and formation of some cubic ice of already quenched droplets. The percentage of crystalline ice further indicates that the temperature of the deposit must have been close to 140 K during continuous droplet deposition because after 37 min at 140 K, 15% of HGW are known to crystallize to cubic ice (read from Fig. 4 in ref. 60).

The average calculated[83,84] and estimated[82,85] cooling rate for vitrification of μm-sized water samples is $\approx 10^6$ to $\approx 10^7 \, K$ s^{-1}. For an average cooling rate of $10^6 \, K \, s^{-1}$, the time needed to cool over 200 degrees is calculated as 0.2 ms.[24] This quenching time is shorter than an empirically determined freezing time of between 0.5 and 1.5 ms for quick-freezing with a liquid-nitrogen-cooled copper block.[88]

The micrometresized water droplets impacting on substrate and deposit are considerably flattened, or spread (cf. Fig. 2(c)). This indicates that before impact the liquid droplets must have been of sufficiently low viscosity to be deformable, and that hyperquenching into the glassy state sets in only after the impact. The HGW samples for Fig. 2 were made with a substrate temperature of 77 K, and thus, the droplets were hyperquenched into the glassy state. For HGW samples made by deposition at 140 K (e.g. for Fig. 5, top) hyperquenching of droplets produces an ultraviscous liquid state.

The spreading of supercooled water drops impacting on ice surfaces was studied by Brownscombe and Hallett[48] and Macklin and Payne[49] (reviewed in ref. 50). They found that the spreading factor, defined as the final maximum drop radius to the initial radius, varied between 1.3 and 6, depending primarily on impact speed and deposit temperature, and that the drops became increasingly flattened with an increase of either of these parameters. The spreading factor read from a

comparison of Fig. 2(a) with 2(c) (that is, parallel *versus* perpendicular cut of the deposit) is ≈ 2–3. Further interpretation of the flattening of hyperquenched droplets, in line with the analysis in ref. 48 and 49, is not meaningful because in the latter case the drops freeze with heat evolution and increase in temperature.

Supercooling of liquid water droplets can occur in supersonic flow already in the gas phase. Bartell *et al.*[89,90] (reviewed in ref. 2) "used evaporative cooling of molecular clusters produced by condensation of water vapour in supersonic flow through small nozzles. Typical cluster sizes and cooling rates were 74 Å (6600 molecules), and 10^7 K s^{-1}, respectively. Electron diffraction patterns of the water clusters showed no evidence of crystallization until roughly 200 K whereupon freezing to ice Ic occurred".[2] Water droplets with ≈ 5 μm diameter used in our experiments for Fig. 5 contain $\approx 2 \times 10^{12}$ water molecules which is $\approx 10^9$ times the number of water molecules used in Bartell's cluster experiments mentioned above. Thus, because of the much larger size of water droplets used in our hyperquenching experiments, the supercooling observed for water clusters cannot simply be assumed here. We conclude that we do not know whether, and to what extent, the μm-sized water droplets are precooled already in the gas phase during supersonic flow, or whether cooling starts only once the droplet hits the cryoplate. This holds only for optimally hyperquenched water droplets, with base pressure of $< 10^{-2}$ mbar (*cf.* experimental section). When the base pressure is $\geq \approx 1$ mbar, mainly crystalline ice is formed.[34] In that case, slow precooling of water droplets already in the gas phase could have contributed to the comparatively low cooling rate and formation of ice.

Vitrification of 0.7 mm thick disks of pure water?

Brower *et al.*[91] recently claimed that 0.7 mm thick disks of pure water can be vitrified on cooling at rates of 110–271 K s^{-1}, by placing one drop of pure liquid water (0.057 cm^3) on a diamond wafer and immersing it in liquid N$_2$. They argued that the high thermal conductivity of the CVD diamond wafer of 14 W/(cm K) used as a "conductive heat-transfer medium allowed cooling rates never before achieved in quenching thick layers of liquid water and revealed that the cooling rate necessary to avoid crystallization of water is far lower than previously expected".[91] Their density value of 1.04 g cm^{-3} for glassy water is now being used in computer modelling studies.[92,93] Brower *et al.*'s claim is in conflict with calculations and measurements of the critical cooling rate necessary to avoid formation of ice (see above). Thus, we need to investigate their evidence for vitrification and formation of glassy water. Their major argument for vitrification is a DSC scan showing on heating a diffuse exotherm over the range of 150–190 K (*cf.* their Fig. 3), whereas the sharp exotherm observable on crystallization of HGW to ice Ic is missing (*cf.* Fig. 4). This sharp crystallization exotherm between 150–160 K during reheating is the one universal feature in all previous studies of the amorphous forms of water.[3] However, their DSC scan resembles that of a sample of μm-sized water droplets hyperquenched on a substrate held at 160 K (*cf.* Fig. 1 in ref. 54). The X-ray diffractogram of this sample indicated formation of disordered ice Ic, and the broad exotherm in the DSC scan had been attributed to annealing effects in ice Ic (discussed in ref. 54). That cubic ice can form from bulk water even at low rates of cooling, has been shown recently by Murray *et al.*[94] As discussed above, even when perfect thermal contact between sample and substrate is achieved by ideal cooling, heat transfer within the water sample limits the cooling rate and the sample thickness which can be vitrified. The crystal growth rate of ice is well known, and it cannot be outwitted by using a diamond wafer as substrate. We conclude that the evidence in ref. 91 is consistent with formation of some disordered crystalline ice,

but not of glassy water (see also ref. 3 for critique and explanation of the transparency of the supposedly glassy water sample of 0.7 mm thickness).

Conclusions

In summary, the DSC results of this study show that hyperquenched water deposited at 140 K behaves as an ultraviscous liquid, with liquid-like relaxation at and below 140 K. This is consistent with the T_g of ≈ 136 K.[4–7] Its limiting structure depends on cooling rate in a manner predicted by theoretical analysis of liquid-to-glass transition,[15,63,65] and it becomes experimentally observable by DSC on subsequent reheating as an increasingly pronounced overshoot with decreasing cooling rate. The effect of cooling rate on the height of the endothermic step disappears when HGW samples are annealed in addition at 130 K, but the T_g value remains the same. Our results contradict Yue and Angell's claim for assignment of HGW's endothermic step to a sub-T_g or "shadow" peak.[9] Yue and Angell[9] emphasize that the onset temperature of "shadow" peaks increases with increasing annealing temperature, and use this as a criterion for their postulated assignment. This effect is not observed here where HGW's T_g remains at ≈ 136 K, independent of whether the sample anneals during deposition at 140 K (*cf.* Fig. 5(a)), or whether it is in addition subsequently annealed at 130 K (Fig. 5(b)). HGW's T_g of ≈ 136 K is consistent with Johari's recent calculation of the dielectric relaxation time of water of 42 ± 14 s at 136 ± 1 K.[13,14] Our DSC study further shows that the previously reported value of HGW's apparent increase in heat capacity (ΔC_p) of 1.6 J K^{-1} mol^{-1} at T_g (ref. 5) must contain a contribution from an overshoot, caused by the annealing procedure, and that the "true" ΔC_p value must be even lower. A lower ΔC_p value is consistent with increasingly "strong" behaviour of deeply supercooled water,[19,20,77,78] and thus, our new data support the proposed fragile-to-strong transition on cooling liquid water from ambient temperature into the deeply supercooled and glassy state.[19–22] Finally, our electron micrographs of HGW deposits show that the droplets are on the whole preserved during hyperquenching, and that they are still liquid when hitting the cryoplate.

References

1   C. A. Angell, *Chem. Rev.*, 2002, **102**, 2627.
2   P. G. Debenedetti, *J. Phys.: Condens. Matter*, 2003, **15**, R1669.
3   C. A. Angell, *Annu. Rev. Phys. Chem.*, 2004, **55**, 559.
4   G. P. Johari, A. Hallbrucker and E. Mayer, *Nature*, 1987, **330**, 552.
5   A. Hallbrucker, E. Mayer and G. P. Johari, *Philos. Mag. B*, 1989, **60**, 179.
6   G. P. Johari, A. Hallbrucker and E. Mayer, *Science*, 1996, **273**, 90.
7   J. P. Johari, A. Hallbrucker and E. Mayer, *J. Chem. Phys.*, 1990, **92**, 6742.
8   V. Velikov, S. Borick and C. A. Angell, *Science*, 2001, **294**, 2335.
9   Y. Yue and C. A. Angell, *Nature*, 2004, **427**, 717.
10 G. P. Johari, *J. Chem. Phys.*, 2002, **116**, 8067.
11 G. P. Johari, *J. Chem. Phys.*, 2003, **119**, 2935.
12 G. P. Johari, *J. Phys. Chem. B*, 2003, **107**, 9063.
13 G. P. Johari, *Phys. Chem. Chem. Phys.*, 2005, **7**, 1091.
14 G. P. Johari, *J. Chem. Phys.*, 2005, **122**, 144508.
15 C. T. Moynihan, A. J. Easteal, M. A. DeBolt and J. Tucker, *J. Am. Ceram. Soc.*, 1976, **59**, 12.

16 C. T. Moynihan, P. B. Macedo, C. J. Montrose, P. K. Gupta, M. A. DeBolt, F. J. Dill, B. E. Dom, P. W. Drake, A. J. Easteal, P. B. Elterman, R. P. Moeller, H. Sasabe and J. A. Wilder, *Ann. NY Acad. Sci.*, 1976, **279**, 15.

17 P. Earis, *Chem. World*, 2005, **2**(4), 23.

18 I. Kohl, L. Bachmann, E. Mayer, A. Hallbrucker and T. Loerting, *Nature*, 2005, **435**, E1.

19 K. Ito, C. T. Moynihan and C. A. Angell, *Nature*, 1999, **398**, 492.

20 S. Sastry, *Nature*, 1999, **398**, 467.

21 F. W. Starr, C. A. Angell and H. E. Stanley, *Physica A*, 2003, **323**, 51.

22 A. Faraone, L. Liu, C.-Y. Mou, C.-W. Yen and S.-H. Chen, *J. Chem. Phys.*, 2004, **121**, 10843.

23 C. A. Tulk, D. D. Klug, R. Branderhorst, P. Sharpe and J. A. Ripmeester, *J. Chem. Phys.*, 1998, **109**, 8478.

24 C. A. Tulk, Y. Ba, D. D. Klug, G. McLaurin and J. A. Ripmeester, *J. Chem. Phys.*, 1999, **110**, 6475.

25 D. D. Klug, C. A. Tulk, E. C. Svensson and C. K. Loong, *Phys. Rev. Lett.*, 1999, **83**, 2584.

26 Y. Suzuki and O. Mishima, *Phys. Rev. Lett.*, 2000, **85**, 1322.

27 Y. Suzuki, *Chem. Phys. Lett.*, 2001, **335**, 357.

28 Y. Suzuki and O. Mishima, *J. Phys. Soc. Jpn.*, 2003, **72**, 3128.

29 W.-H. Kim, M. McPhillen, J. M. Hayes and G. J. Small, *Chem. Phys. Lett.*, 1993, **207**, 443.

30 W.-H. Kim, T. Reinot, J. M. Hayes and G. J. Small, *J. Phys. Chem.*, 1995, **99**, 7300.

31 T. Reinot, W.-H. Kim, J. M. Hayes and G. J. Small, *J. Chem. Phys.*, 1996, **104**, 793.

32 W.-H. Kim, T. Reinot, J. M. Hayes and G. J. Small, *J. Chem. Phys.*, 1996, **104**, 6415.

33 C. A. Angell, Y. Yue, L.-M. Wang, J. R. D. Copley, S. Borick and S. Mossa, *J. Phys.: Condens. Matter*, 2003, **15**, S1051.

34 E. Mayer, *J. Appl. Phys.*, 1985, **58**, 663.

35 P. Brüggeller and E. Mayer, *Nature*, 1980, **288**, 569.

36 J. Dubochet and A. W. McDowall, *J. Microsc.*, 1981, **124**, RP3.

37 E. Mayer and P. Brüggeller, *Nature*, 1982, **298**, 715.

38 G. M. Hidy, *Aerosols. An Industrial and Environmental Science*, Academic Press, New York, 1984.

39 E. Mayer, *J. Phys. Chem.*, 1985, **89**, 3474.

40 J. B. Anderson, in 1*Molecular Beams from Nozzle Sources*, ed. P. P. Wegener, New York, 1974.

41 M. A. D. Fluendy and K. P. Lawley, *Chemical Applications of Molecular Beam Scattering*, Chapman and Hall, London, 1972.

42 W. Hage, A. Hallbrucker and E. Mayer, *J. Chem. Soc., Faraday Trans.*, 1996, **92**, 3183.

43 P. Brüggeller and E. Mayer, *J. Phys. Chem.*, 1981, **85**, 4135.

44 E. L. Benedetti and P. Favard, *Soc. Fr. Microsc. Electr.*, 1973.

45 L. Bachmann, in *Freeze-Etching of Dispersions, Emulsions and Macromolecular Solutions of Biological Interest*, ed. R. A. Steinbrecht and K. Zierold, Springer, Berlin, 1987.

46 L. Bachmann and W. W. Schmitt, *Proc. Natl. Acad. Sci. USA*, 1971, 2149.

47 K. R. Wilson, R. D. Schaller, D. T. Co, R. J. Saykally, B. S. Rude, T. Catalano and J. D. Bozek, *J. Chem. Phys.*, 2002, **117**, 7738.

48 J. L. Bronswcombe and J. Hallett, *Q. J. R. Meterol. Soc.*, 1967, **93**, 455.

49 W. C. Macklin and G. S. Payne, *Q. J. R. Meteorol. Soc.*, 1968, **94**, 167.

50 H. R. Pruppacher and J. D. Klett, in *Microphysics of Clouds and Precipitation*, Reidel, Dordrecht, 1980.

51 J. E. Field, *Wear*, 1999, **1**, 233–235.

52 A. Hallbrucker and E. Mayer, *J. Phys. Chem.*, 1987, **91**, 503.

53 A. Hallbrucker, E. Mayer and G. P. Johari, *J. Phys. Chem.*, 1989, **93**, 4986.

54 I. Kohl, E. Mayer and A. Hallbrucker, *Phys. Chem. Chem. Phys.*, 2000, **2**, 1579.

55 E. Mayer, *J. Phys. Chem.*, 1986, **90**, 4455.

56 G. P. Johari, S. Ram, G. Astl and E. Mayer, *J. Non-Cryst. Solids*, 1990, **116**, 282.

57 S. Ram and G. P. Johari, *Phil. Mag.*, 1990, **61**, 299.

58 I. M. Hodge, *J. Non-Cryst. Solids*, 1994, **169**, 211.

59 L. C. E. Struik, *Physical Aging in Amorphous Polymers and Other Materials*, Elsevier, Amsterdam, 1978.

60 W. Hage, A. Hallbrucker, E. Mayer and G. P. Johari, *J. Chem. Phys.*, 1994, **100**, 2743.

61 C.A. Angell and L. M. Torrell, *J. Chem. Phys.*, 1983, **78**, 937.

62 A. J. Easteal, J. A. Wilder, R. K. Mohr and C. T. Moynihan, *J. Am. Ceram. Soc.*, 1977, **60**, 134.

63 M. A. DeBolt, A. J. Easteal, P. B. Macedo and C. T. Moynihan, *J. Am. Ceram. Soc.*, 1976, **59**, 16.

64 H. N. Ritland, *J. Am. Ceram. Soc.*, 1954, **37**, 370.

65 G. P. Johari, A. Hallbrucker and E. Mayer, *J. Phys. Chem.*, 1989, **93**, 2648.

66 B. Wunderlich, *Thermal Analysis*, Academic Press, New York, 1990.

67 R. J. Speedy, *J. Phys. Chem.*, 1992, **96**, 2322.

68 G. P. Johari, G. Fleissner, A. Hallbrucker and E. Mayer, *J. Phys. Chem.*, 1994, **98**, 4719.

69 G. P. Johari, *Philos. Mag.*, 1977, **35**, 1077.

70 G. P. Johari, *Chem. Phys.*, 2000, **258**, 277.

71 G. P. Johari, *J. Chem. Phys.*, 2000, **112**.

72 G. P. Johari, *J. Chem. Phys.*, 1993, **98**, 7324.

73 R. S. Smith and B. D. Kay, *Nature*, 1999, **398**, 788.

74 R. J. Speedy, P. G. Debenedetti, R. S. Smith, C. Huang and B. D. Kay, *J. Chem. Phys.*, 1996, **105**, 240.

75 R. S. Smith, C. Huang and B. D. Kay, *J. Phys. Chem. B*, 1997, **101**, 6123.

76 R. S. Smith, Z. Dohnalek, G. A. Kimmel, K. P. Stevenson and B. D. Kay, *Chem. Phys.*, 2000, **258**, 291.

77 C. A. Angell, *J. Non-Cryst. Solids*, 1988, **102**, 205.

78 P. G. Debenedetti, *Metastable Liquids*, Princeton University Press, 1996.

79 C. A. Angell and J. C. Tucker, *J. Phys. Chem.*, 1980, **84**, 268.

80 A. Minoguchi, R. Richert and C. A. Angell, *Phys. Rev. Lett.*, 2004.

81 R. C. Ruhl, *Mater. Sci. Eng.*, 1967, **1**, 313.

82 L. Bachmann and E. Mayer, in *Physics of Water and Ice: Implications for Cryofixation*, ed. R. A. Steinbrecht and K. Zierold, Springer, Berlin, 1987.

83 D. R. Uhlmann, *J. Non-Cryst. Solids*, 1972, **7**, 337.

84 W. B. Bald, *J. Microsc.*, 1986, **143**, 89.

85 E. Mayer, *J. Am. Chem. Soc.*, 1994, **116**, 10571.

86 J. Dubochet, M. Adrian, J.-J. Chang, J.-C. Homo, J. Lepault, A. McDowall and P. Schultz, *Q. Rev. Biophys.*, 1988, **21**, 129.

87 W. Hage, A. Hallbrucker, E. Mayer and G. P. Johari, *J. Chem. Phys.*, 1995, **103**, 545.

88 P. H. W. W. Baatsen, *J. Microsc.*, 1993, **172**, 71.

89 L. S. Bartell and J. Huang, *J. Phys. Chem.*, 1994, **98**, 7455.

90 J. Huang and L. S. Bartell, *J. Phys. Chem.*, 1995, **99**, 3924.

91 J. Brower, W. E. D. J. Schedgick and L. K. Bigelow, *J. Phys. Chem. B*, 2002, **106**, 4565.

92 I. Brovchenko, A. Geiger and A. Oleinikova, *J. Chem. Phys.*, 2003, **118**, 9473.

93 I. Brovchenko and A. Geiger, A. Oleinikova, *Condens. Matter*, 2005, arXiv:cond-mat/0503584.

94 B. J. Murray, D. A. Knopf and A. K. Bertram, *Nature*, 2005, **434**, 202.